Characterization of 3D Printed Re-Entrant Chiral Auxetic Geometries

Tatheer Zahra

Abstract—Auxetic materials have counteractive properties due to re-entrant geometry that enables them to possess Negative Poisson's Ratio (NPR). These materials have better energy absorbing and shock resistance capabilities as compared to conventional positive Poisson's ratio materials. The re-entrant geometry can be created through 3D printing for convenient application of these materials. This paper investigates the mechanical properties of 3D printed chiral auxetic geometries of various sizes. Small scale samples were printed using an ordinary 3D printer and were tested under compression and tension to ascertain their strength and deformation characteristics. A maximum NPR of -9 was obtained under compression and tension. The re-entrant chiral cell size has been shown to affect the mechanical properties of the re-entrant chiral auxetics.

Keywords—Auxetic materials, 3D printing, Negative Poisson's Ratio, re-entrant chiral auxetics.

I. INTRODUCTION

AUXETIC materials are often called meta-materials because of their geometrical configuration and ability to be manufactured through various methods such as thermo-mechanical process, 3D printing, weaving and additive manufacturing process [1]-[4]. The auxetic behavior refers to an ability to expand laterally while stretched longitudinally or contract laterally when compressed in the longitudinal direction. This property enables auxetic materials to exhibit NPR. A common auxetic geometry is a re-entrant geometry that facilitates this behavior as shown in Fig. 1. Due to NPR behavior, these materials can absorb shock energy effectively and have improved indentation and stab resistance.
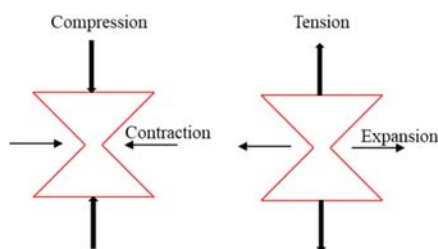

Fig. 1 Re-entrant micro-structure of auxetics

Auxetic materials have been employed in many industries including defense [5], biomedical [6], sports [7] and automobiles [8] as shock absorbers, support membranes and protective foams. Three-dimensional printing technique to manufacture these materials has been shown convenient with an opportunity of changing cell sizes, shapes and materials [2]. Common shapes that have been printed and tested earlier are regular honeycomb, re-entrant auxetic honeycomb [9], [10], chiral honeycomb [4], tetra chiral honeycomb and anti–tetra chiral honeycomb [11]. All these shapes were found superior in strength, energy absorbing, and impact resistance as compared to their conventional counterparts printed with non-auxetic geometries.

Re-entrant chiral auxetic (RCA) geometries which combine aspects of both re-entrant and chiral honeycomb microstructures were first introduced by Alomarah et al. [11], [12]. They tested this geometry through finite element analysis and then manufacture them through a Multi Jet Fusion (MJF) 3D printing technology using polyamide12 (PA12) a general-use plastic which is known for its tensile strength, toughness, impact strength and ability to flex without fracture. This geometry showed high strength and specific energy absorption which was equivalent to tetra chiral honeycomb shape and had the highest absolute value of NPR of -2.5.

Materials which have been trialed to print 3D auxetic shapes include acrylonitrile butadiene styrene (ABS), PA12, polylactic acid (PLA), polyethylene terephthalate glycol modified (PETg), Tangoplus (silicone-based rubber material), Thermoplastic polyurethane (TPU) and Aluminum (Al). The selection of material is mainly depended on the application and the type of printers available in the labs. As expected, the metallic auxetics showed high strength and stiffness as compared to the polymer based auxetics whereas, the polymer based printed auxetics have more flexibility and are preferred in the fields of biomedical, sports and other applications. However, with innovation in polymers such as fiber reinforced polymers it is possible to create high strength and high stiffness auxetic geometries [13]. Overall, 3D printing of auxetic materials is a developing area of research and needs more investigations.

The objective of this paper is to study the effect of cell size of RCA auxetic geometries on their strength, stiffness and Poisson's ratio. The compressive and tensile properties of RCA auxetic geometries with three different cell sizes are presented in this paper. The RCA geometries were printed in a conventional 3D printer using PLA filament at Queensland University of Technology (QUT) and were tested under static compression and tension. The results were studied in terms of failure modes, stress-strain curves and Poisson's ratio variation.

Tatheer Zahra is with the Queensland University of Technology (QUT), Brisbane, QLD 4000 Australia (phone: +61731385327; e-mail: t.zahra@qut.edu.au).

World Academy of Science, Engineering and Technology
International Journal of Materials and Metallurgical Engineering
Vol:15, No:5, 2021

II. PRINTING AND TESTING OF RCA GEOMETRIES

Computer-aided drafting (CAD) was employed to develop the RCA geometry. A typical cell is shown in Fig. 2 and the corresponding dimensions adopted for the three different cell sizes are listed in Table I.
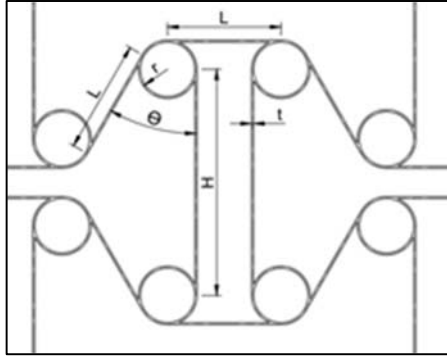

Fig. 2 Single cell of RCA geometry

TABLE I
RCA CELL GEOMETRIC PARAMETERS

Structure	Height, H mm	Length, L mm	Angle, θ deg	Thickness, t mm
RCA-1	20	10.0	30	2
RCA-2	25	12.5	30	2
RCA-3	30	15.0	30	2

The designed samples consisted of three cells with overall dimensions of 56 mm (wide) × 82 mm (long) for RCA-1, 66 mm (wide) × 99 mm (long) for RCA-2 and 76 mm (wide) × 115 mm (long) for RCA-3. The thickness of all types of RCA samples was 10 mm for tension tests and 20 mm for compression tests. The increase of thickness was deliberate to avoid buckling failure under compression loading. The specimens for tension tests were manufactured with protrusions on the top and bottom to accommodate the samples in the grips of the testing machine.

For printing, PLA filament was adopted due to ease of printing and low cost [14]. The samples were manufactured using a Lulzbot TAZ 5/6 3D printer. Typical 3D printed samples are shown in Fig. 3.
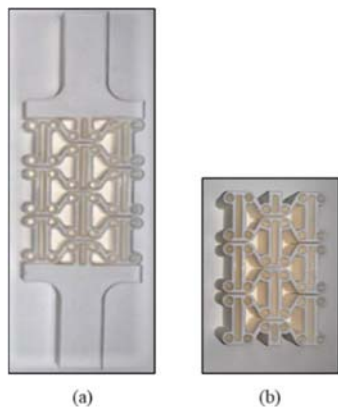

Fig. 3 Typical 3D printed RCA samples for (a) tension and (b) compression tests

The printed specimens were tested under monotonic compression and tension loads using an INSTRON machine with a load cell capacity of 50 kN. A uniform displacement at the rate of 1 mm/min was applied to ascertain the stress-strain properties. A total of 18 specimens were tested which consisted of three samples for each type of RCA geometries under compression and tension loads separately. ASTM D 638: 2014 [15] standards and ASTM D 695: 2015 [16] were followed for tension and compression testing, respectively.
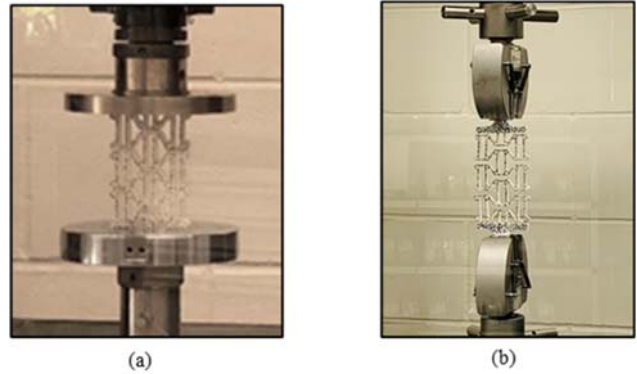

Fig. 4 Testing of RCA samples (a) compression (b) tension

III. EXPERIMENTAL RESULTS

The test results were studied in the form of failure modes, measured strengths, stress strain curves and Poisson's ratio variation. These results are discussed in the following sub-sections.

A. Failure Modes

Under compressive loads, all RCA geometries show a similar failure mode with buckling of vertical cells and collapsing of gaps between the re-entrant cells. A typical failure mode under compression is shown in Fig. 5 (a). As shown in this figure, the RCA geometry contracted laterally under longitudinal compressive load which resulted in an NPR behavior. The decreases in the lateral dimensions were 2.8 mm, 5.9 mm and 6.8 mm for the RCA-1, RCA-2 and RCA-3, respectively. These lateral dimensions were measured just before failure occurred by fracturing of cells using a digital camera image analysis. The lateral deflection was highest in the RCA-3 geometry due to larger cell size, while RCA-1 showed the lowest lateral deflection due to smallest cell size.

When subjected to tensile loads, the RCA geometries expand in all directions until failure due to rupture of the middle cell. Typical failure mode in tension to represent all types of RCA geometries is shown in Fig. 5 (b). The maximum lateral expansion in RCA-1 samples was 5.4 mm, RCA-2 was expanded by 6.5 mm and RCA-3 by 8.1 mm. The larger the cell size, higher was the lateral deflection at the mid height of the specimens.

B. Strength

The mean ultimate strength and strain at failure in compression and tension of all RCA specimens are shown in Table II. The respective coefficient of variation (COV) is also

World Academy of Science, Engineering and Technology
International Journal of Materials and Metallurgical Engineering
Vol:15, No:5, 2021

given in parentheses. These results clearly show that the small cell size resulted in a high strength under tension as well as compression. RCA-1 showed the highest compression and tension strength which were found about 60% higher than RCA-3 and 30% higher than RCA-2. The closer cell geometry provides stability to the RCA structures and thus resulted in a high strength. Conversely, the ultimate strain, which was measured after the peak load dropped by 20% in all the samples, had a reverse trend. Bigger RCA cells provided larger deformation and strain. The failure strain in compression was smaller as compared to what was measured in tension due to expansion of RCA geometry whereas, under compression, the cells buckled, and gaps collapsed with no space available to deform further and ultimately ruptured.
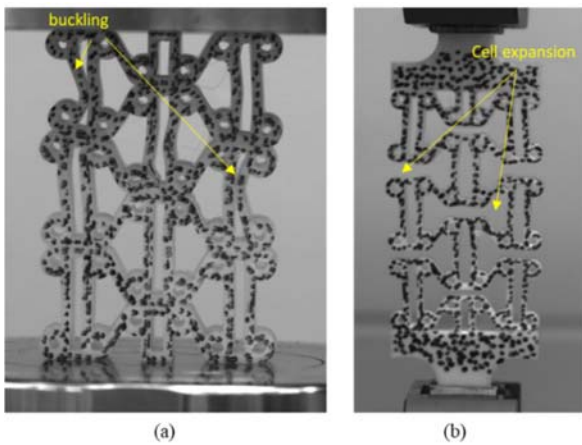

Fig. 5 Typical failure mode of RCA samples for (a) compression and (b) tension tests

TABLE II
ULTIMATE STRENGTH AND STRAIN OF RCA GEOMETRIES

Structure	Compressive strength MPa	Ultimate compressive strain (mm/mm)	Tensile strength MPa	Ultimate tensile strain (mm/mm)
RCA-1	46 (0.5%)	0.05 (4.3%)	1.30 (14%)	0.098 (8.8%)
RCA-2	35 (1.1%)	0.08 (7.5%)	0.83 (1.9%)	0.096 (5.6%)
RCA-3	17.4 (3.5%)	0.09 (10.1%)	0.58 (2.2%)	0.10 (9.1%)

C. Stress-Strain Curves

The representative compressive stress-strain curves of RCA geometries are shown in Fig. 6. Three distinct zones can be seen in all types of RCA samples. The initial portion of the curves with a lower slope due to collapsing of the gaps between the RCA cells and did not cause increase in the loads. When all gaps are collapsed, the material stiffening occurred with increase in slope and strength. Finally, after peak strength, the post-peak response is due to excessive buckling of cells and then rupturing. RCA-1 showed the highest compressive strength, but the lowest deformability as can be seen by the lowest failure strain. RCA-3 was the weakest with the highest deformability characteristics.

The stress-strain curves of RCA geometries under tensile loading are shown in Fig. 7. In tension also, the highest strength was measured for the RCA-1 which had the smaller cell sizes. In addition, there is a sudden drop in the peak strength due to

cracking in the cells, after which the sample continues to deform and exhibited hardening. RCA-2 and RCA-3 did not exhibit such behavior and strain gaining is nonlinear and gradual in both of these RCA types. The overall deformability or the ultimate failure strain was quite similar in all types of RCA. The tensile strength was determined much lower than the compressive strength. The tensile strength was found only 3% of the compressive strength for almost all RCA geometries.
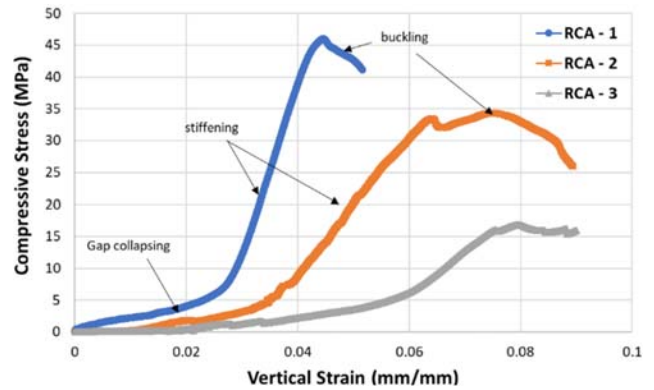

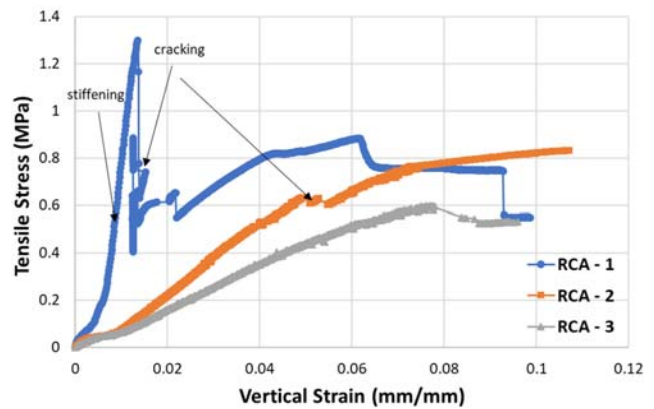Fig. 6 Compressive stress-strain curves of RCA geometries

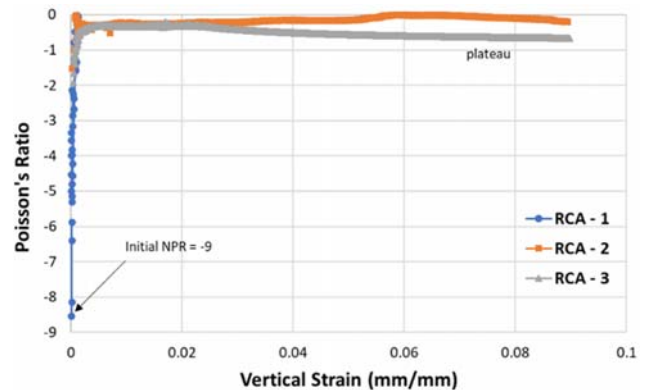Fig. 7 Tensile stress-strain curves of RCA geometries

Fig. 8 Poisson's ratio variation under compression

D. Poisson's Ratio Variation

Poisson's ratio is an important parameter for auxetic geometries. The Poisson's ratio was calculated at regular intervals from the strain calculated from the digital images. The

World Academy of Science, Engineering and Technology
International Journal of Materials and Metallurgical Engineering
Vol:15, No:5, 2021

variation of Poisson's ratio with the longitudinal vertical strain is shown in Fig. 8 for the compression tests. An initial NPR of around -9 was obtained under elastic range which was reduced to a plateau with an average NPR of -0.3 until failure.

For tension, a similar variation of Poisson's ratio was recorded as shown in Fig. 9. The initial Poisson's ratio was -9 which reduced to -0.13 on an average after the elastic range was passed. All geometries continuously showed NPR throughout the loading regime. This property is useful in providing energy abruption and better bonding with other materials.
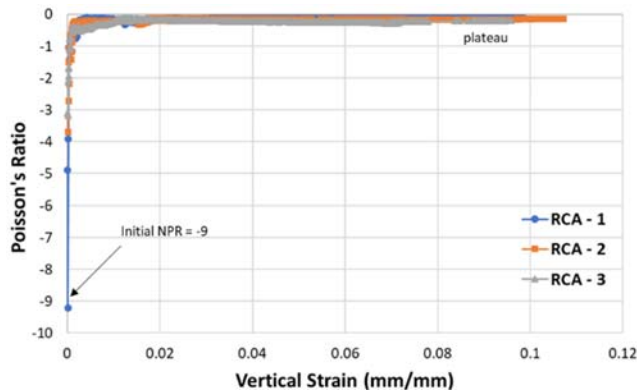

Fig. 9 Poisson's ratio variation under tension

IV. CONCLUSION

The mechanical properties of 3D printed RCA have been investigated in this research. Three types of geometries were developed for different cell sizes using an ordinary printer with a PLA filament. The geometries were tested under compression and tension loads. Following are the main conclusions from this research.

1. The cell size of the RCA geometries affects their strength and deformation characteristics. The smaller cell size resulted in a higher tensile and compressive strength but a lower ultimate strain magnitude.
2. The highest compression strength was obtained as 46 MPa for RCA-1 with a 20 mm cell size.
3. The maximum tensile strength was observed as 1.3 MPa for RCA-1 geometries.
4. The maximum Poisson's ratio was measured as -9 under compression and tension again for RCA-1 that had the cell size of 20 mm.
5. The failure in compression occurred due to collapsing of gaps between the cells and then buckling of vertical members in the cells.
6. The failure in tension was caused by cracking in the geometries that ultimately resulted in rupture of the specimens.

In summary, the characterized RCA geometries in this paper advance knowledge in 3D printed auxetics made of PLA polymer by comparing their tension and compression properties. The effect of cell size was also evaluated, and it was determined that the smaller cell size provided stiffness and strength to the RCA geometries. In future, these geometries can be further studied for different materials, energy absorption capabilities and their application in protective equipment.

REFERENCES

[1] T. Zahra and M. Dhanasekar, "Characterization of cementitious polymer mortar – Auxetic foam composites," *Construction and Building Materials*, 2017, vol. 147, pp. 143–159.
[2] T. Li, Y. Chen and X. Hua et al., "Exploiting negative Poisson's ratio to design 3D-printed composites with enhanced mechanical properties," *Materials and Design*, 2018, vol. 142, pp. 247–258.
[3] E.C. Yang, T.D. Ngo, D. Ruan and P. Tran, "Impact Resistance and Failure Analysis of Plain-Woven Curtains," *International Journal of Protective Structures*," 2015, vol. 6, pp. 113-136.
[4] A. Alomarah, D. Ruan, S. Masood and Z. Gao, "Compressive properties of a novel additively manufactured 3D auxetic structure," *Smart Materials and Structures*, 2019, vol. 17, 085019.
[5] M. Mir, M. Ali, J. Sami and U. Ansari, "Review of Mechanics and Applications of Auxetic Structures," *Advances in Materials Science and Engineering*, 2014, pp. 1-17.
[6] M. Sanami, "Auxetic materials for biomedical applications," *PhD thesis*, University of Bolton, 2015.
[7] O. Duncan and T. Shepherd et al., "Review of Auxetic Materials for Sports Applications: Expanding Options in Comfort and Protection," *Applied Sciences*, 2018, vol. 8(6), 941.
[8] G. Qiang, Q. Gao and L. Wang, "Dynamic Crushing Behaviors of Four Kinds of Auxetic Structures," *SAE Technical Paper* 2019-01-1096, 2019.
[9] X. Hou, Z. Deng and K. Zhang, "Dynamic Crushing Strength Analysis of Auxetic Honeycombs," *Acta Mechanica Solida Sinica*, 2016, vol. 29(5), pp. 490-501.
[10] X. Wang, B. Wang, X. Li, and L. Ma, "Mechanical properties of 3D re-entrant auxetic cellular structures," *International Journal of Mechanical Sciences*, 2019, vol. 131-132, pp. 396-407.
[11] A. Alomarah, S. H. Masood, I. Sbarski, B. Faisal, Z. Gao and D. Ruan, "Compressive properties of 3D printed auxetic structures: experimental and numerical studies," *Virtual and Physical Prototyping*, 2020, vol. 15:1, pp. 1-21.
[12] A. Alomarah, D. Ruan, and S. Masood, "Tensile properties of an auxetic structure with re- entrant and chiral features—a finite element study," *The International Journal of Advanced Manufacturing Technology*, vol. 99(9-12), pp. 2425-2440.
[13] K. Essassi, J. Rebiere, A. El Mahi, M. A. Ben Souf, A. Bouguecha, M. Haddar, "Experimental and analytical investigation of the bending behaviour of 3D-printed bio-based sandwich structures composites with auxetic core under cyclic fatigue tests," *Composites Part A: Applied Science and Manufacturing*, 2020, vol. 131, 105775.
[14] All3DP, "PLA vs ABS – Filaments for 3D Printing Compared", March 20, 2019. https://all3dp.com/1/pla-vs-abs-filament-3d-printing/#section-material-comparison.
[15] ASTM D 638, "Standard Test Method for Tensile Properties of Plastics," 2014.
[16] ASTM D 695, "Standard Test Method for Compressive Properties of Rigid Plastics," 2015.

Tatheer Zahra was born in Pakistan and received her engineering education from NED University of Engineering and Technology, Pakistan. She was awarded a PhD scholarship by Queensland University of Technology (QUT), Australia, from where she completed her PhD in structural engineering in 2017. Her PhD research was based on masonry and high energy absorbing composites for structural protection. She was awarded a high achiever award in higher degree education in 2017 from QUT.

World Academy of Science, Engineering and Technology
International Journal of Materials and Metallurgical Engineering
Vol:15, No:5, 2021

She is working as a lecturer in the School of Civil and Environmental Engineering at Queensland University of Technology (QUT) since 2018. She has six years of research experience in structural masonry and auxetic materials. She has been investigating the performance of interlocking mortarless masonry under various loading conditions in comparison to the conventional mortared masonry. She developed new genre auxetic materials and mortar based auxetic composites to provide protection and enhance the performance of masonry and concrete structures under impact and various other load conditions.

Dr. Zahra is a member of Engineers Australia and Pakistan Engineering Council. She is also a chief investigative member in BD-004-19 committee of Standards Australia for developing guidelines of Mortarless masonry.